

## Article

# A Route towards Durable Underwater Stable Superhydrophobic Surfaces: PET-Reinforced Candle Soot Layers

Xinghua Wu \*, Zhaokang Han , Yuchao Wang, Yutong Pan and Xiaohua Jie

School of Materials and Energy, Guangdong University of Technology, Guangzhou 510006, China; laohutu985@163.com (Z.H.); chao982630582@163.com (Y.W.); panyt1998@163.com (Y.P.); jiejxh@gdut.edu.cn (X.J.)  
\* Correspondence: wuxi0011@e.ntu.edu.sg

**Abstract:** Superhydrophobic coating is widely used due to its waterproof and self-cleaning properties. Carbon soot (CS) nanoparticles are naturally superhydrophobic and non-toxic which are superior to other superhydrophobic coating. However, the weak binding force of the CS nanoparticle layers hinders their practical application. In this study, micro-nanostructured PET-CS superhydrophobic coatings were prepared by a simple method. The obtained coatings presented durable superhydrophobicity and underwater stability, which are superior to PDMS-CS coatings and CS layers. The coating surfaces demonstrated superhydrophobicity under a water pressure of 13.72 kPa for up to 16 days. The surface could withstand water flush for more than 15 min. The coatings also demonstrated good mechanical stability and maintained superhydrophobicity after an abrasion length of 8 m. The stable long-lasting underwater superhydrophobic surface is of great importance for marine applications.

**Keywords:** superhydrophobic; candle soot; mechanical stability; underwater stability; micro-nanostructure



**Citation:** Wu, X.; Han, Z.; Wang, Y.; Pan, Y.; Jie, X. A Route towards Durable Underwater Stable Superhydrophobic Surfaces: PET-Reinforced Candle Soot Layers. *Surfaces* **2024**, *7*, 225–237. <https://doi.org/10.3390/surfaces7020015>

Academic Editor: Aleksey Yerokhin

Received: 1 December 2023

Revised: 21 January 2024

Accepted: 20 March 2024

Published: 2 April 2024



**Copyright:** © 2024 by the authors. Licensee MDPI, Basel, Switzerland. This article is an open access article distributed under the terms and conditions of the Creative Commons Attribution (CC BY) license (<https://creativecommons.org/licenses/by/4.0/>).

## 1. Introduction

Engineered wettability is a key issue used to modify the solid–liquid interactions and plays an important role in designing various functional surfaces and devices for many practical applications. Contact angle and roll-off angle measurement is a qualitative way to evaluate surface wettability, including superhydrophilic, hydrophilic, superhydrophobic, and hydrophobic characteristics. A superhydrophobic surface is of great significance in the fields of industrial chemistry, oil technology, and agriculture. However, the underwater metastability of trapped air bubbles hinders the durability and practical application of superhydrophobic surfaces. Superhydrophobicity, especially for an underwater situation against harsh environmental conditions, is urgently required in marine engineering and offshore constructions. Marmur [1] formulated thermodynamic equilibrium and stability conditions and found that underwater superhydrophobicity may be feasible and thermodynamically stable with sufficiently high roughness ratios. Yu et al. [2] simulated a theoretical model to predict the fate of plastrons of superhydrophobic surfaces underwater in high-speed flow. A range of well-defined superhydrophobic surfaces attached underneath a motorboat were experimentally tested in seawater. Smyrnakis et al. [3] found that plasma micro-nanotextured superhydrophobic surfaces could retain underwater superhydrophobicity for at least 60 days. Xiang et al. [4] examined the ultimate stable states on superhydrophobic surfaces and proved the existence of an ultimate stable state on underwater superhydrophobic surfaces. Breveleri et al. [5] experimentally investigated the capability of gas injection to restore the plastron on an underwater superhydrophobic porous material from a fully wetted state. Xiang et al. [6] prepared biomimetic artificial *Salvinia* surfaces using 3D printing technology and successfully achieved the recovery of the air mattress. Choi et al. [7] fabricated superhydrophobic surfaces with re-entrant structures of different Young's moduli (E). Deepak and Arindam [8] fabricated superhydrophobic surfaces with highly re-entrant geometry and hierarchical surface morphology.

The surfaces showed increased longevity of the plastron layer at different pressures and temperatures. Dai et al. [9] reported a facile approach to fabricate a superhydrophobic and anti-corrosion strain sensor for robust underwater applications. Ni et al. [10] built a robust superhydrophobic multifunctional rGO/PPy/poly(dimethylsiloxane) polyurethane sponge sensor for the underwater detection of pressure, water level, and temperature. An underwater stable superhydrophobic surface has long been desired but is susceptible to the diffusion of air in water, mechanical damage, and toxic fluorine-containing reagents.

Candle soot (CS) particles, as green and sustainable materials with high hydrophobicity and high stratification dimensions, are fluorine-free and low-cost. Efforts were made to use amorphous carbon soot as a filler. Bandosz et al. [11] first reported a kind of magnetic soot which possesses a high adsorption capacity and an easiness of mechanical separation in removing oil contamination from water. Currently, superhydrophobic soot can even be applied to in vitro fertilization analyses [12]. Yuan et al. [13,14] prepared a flexible carbon fabric via a simple and low-cost flame synthesis process using ethanol as a soot precursor. Iqbal and Majhy [15] prepared a stable and biocompatible superhydrophobic and superoleophobic surface from polydimethylsiloxane (PDMS) and CS. Zhao et al. [16] obtained superhydrophobic and superoleophilic nickel foam by loading a soot layer onto commercial nickel foam. Do et al. [17] fabricated a robust superhydrophobic micro-nano hierarchical surface using compression molding with CS nanoparticles and a thermoplastic polymer. Esmeryan et al. [18] utilized a specially designed aluminum chimney, mounted over an ignited paper-based wick immersed in rapeseed oil, and obtained dense and fused carbon chains on the substrate surface. The modified carbon coating maintained superhydrophobicity up to  $\sim 300$  °C and presented enhanced surface adhesion and mechanical durability under random water flows. Liu [19] reported transparent superhydrophobic surfaces by calcining CS-coated PDMS films. The coating displayed a water contact angle of  $163^\circ$  and a roll-off angle of about  $1^\circ$ . Celik et al. [20] developed a robust water impact-resistant all-organic superhydrophobic coating from a colloidal dispersion composed of carnauba wax and CS. The coated surfaces presented superhydrophobicity with a water contact angle of  $172^\circ$  and a roll-off angle of  $3^\circ$ , retaining superhydrophobicity even after 400 cycles of continuous water spraying with an impact pressure of 7.4 kPa. The fabrication of effective and low-cost underwater stable superhydrophobic coatings for marine applications is a worldwide challenge; therefore, a feasible method to fabricate a mechanically durable and underwater stable superhydrophobic coating is highly required. To our knowledge, no study has been carried out to examine the effect of polyethylene terephthalate (PET) powders on the improvement in the durability of CS networks.

In this study, the desired CS networks with superhydrophobicity were fastened with PET, which presents high stiffness and high strength and is highly resistant to moisture and organic materials. The obtained PET-CS surface was characterized based on its morphology, wetting properties, underwater stability, mechanical properties, and chemical durability. The coating surfaces displayed good underwater stability and mechanical/chemical durability, which is superior to the PDMS-CS coatings.

## 2. Experimental Section

### 2.1. Materials

PET powders (99.9%, 100  $\mu\text{m}$ ) were obtained from Shanghai Aladdin Reagent Co., Ltd. (Shanghai, China). PDMS was obtained from Dow Corning Co., Ltd. (Singapore) Ethanol (99.7%) and glass slides ( $76.2 \times 25.4 \times 1$  mm) were purchased from Guangzhou Chemical Reagent Factory (Guangzhou, China). Candles (wax, radius: 0.8 cm) were purchased from local stores.

### 2.2. Methods

#### 2.2.1. Preparation of CS Surface

The CS layers were obtained by placing cleaned glass slides above the candle flame for 60 s. The detailed method was consistent with our previous reports [21]. In detail, the

PET powder-adhered samples were placed above a candle at a distance of 2 cm and moved back and forth for 90 s. The obtained CS networks were labeled as CS.

### 2.2.2. Preparation of PDMS-CS Composite Coatings

Firstly, 10 mL of PDMS base and 1 mL of PDMS curing agent were mixed via magnetic stirring at a speed of 300 r/min for 10 min. Secondly, the mixture was uniformly sprayed onto the preheated glass substrates with an air gun. The distance between the spray gun and the glass substrate was kept at about 8 cm. After that, the CS networks were deposited from a candle flame followed by a repetition of Section 2.2.1. Finally, the samples were heated at 100 °C for 15 min. The obtained samples were labeled as PDMS-CS.

### 2.2.3. Preparation of PET-CS Composite Coatings

Firstly, 0.1 mL of ethanol was evenly dropped onto the glass substrate, forming a uniform liquid layer. 5 g of PET powders were evenly spread over the liquid layer using a 150-mesh sieve before the ethanol evaporated. The PET powders temporarily adhered to the glass substrate due to the surface tension of the liquid layer. Secondly, carbon soot layers were deposited from a candle flame followed by a repetition of the procedure in Section 2.2.1. The obtained samples were labeled as PET-CS. To remove the weakly bonded candle soot particles, the PDMS-CS and PET-CS samples were cleaned under a high-speed flow of running water (4 m/s) for several minutes.

## 2.3. Characterization

The surface morphology of the samples was scanned by a field emission scanning electron microscope (FESEM, Hitachi Co., Ltd., SU8010, Tokyo, Japan). The water contact angle (WCA) and roll-off angle (RA) of the samples were measured by the fully automatic contact angle measuring and contour analysis system (Dataphysics, OCA100, Filderstadt, Germany). The droplet volumes used for the WCA and RA measurements were 5  $\mu$ L and 10  $\mu$ L, respectively. The water wettability tests were carried out for 5 specimens of each sample. Five random positions of each specimen were measured.

To evaluate the underwater stability of the coatings, a self-designed glass tube with a diameter of 8 cm and a height of 160 cm was employed and filled with deionized water [21]. The samples were immersed in the tube for 30 days at different depths of 40 cm (hydrostatic pressure 3.92 kPa) and 140 cm (hydrostatic pressure 13.72 kPa), respectively, as shown in Figure 1. At the same time, the WCA and RA of the samples were measured every 24 h.

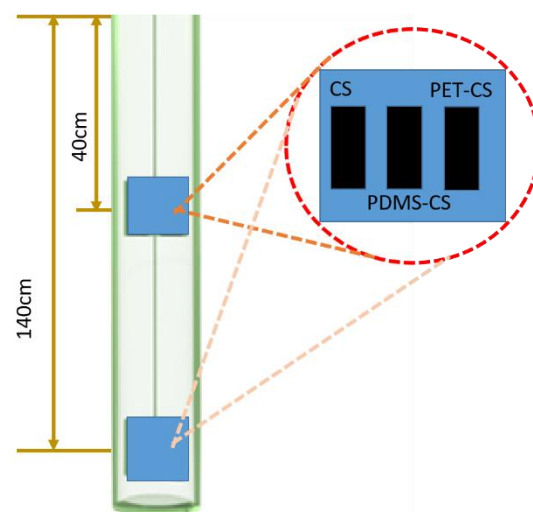


**Figure 1.** Schematic diagram of underwater stability test.

To investigate the mechanical stability of the samples, the coatings were scratched with sandpaper [21]. Samples with dimensions of 2.5 cm  $\times$  4.0 cm were scratched against

sandpaper (400#) at a speed of 1 cm/s under a load of 100 g as shown in Figure 2. The samples were moved back and forth for 20 cm as an abrasion cycle. The change in the WCA of the samples was recorded in every cycle.

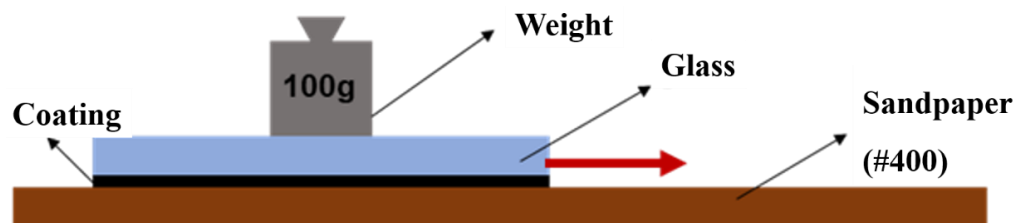


**Figure 2.** Schematic diagram of sandpaper abrasion test. The red arrow indicates the sample moving direction.

The water impact test was conducted following the previous report [9]. Figure 3 shows a schematic illustration of the water impact test. Samples with the coated side facing up were placed under a water jet at a tilt angle of 45 degrees. Running water flowed over the coating surfaces at a height of 20 cm with a flow rate of 2 m/s. The change in the WCA of the surfaces with the impact time of the water flow was recorded.

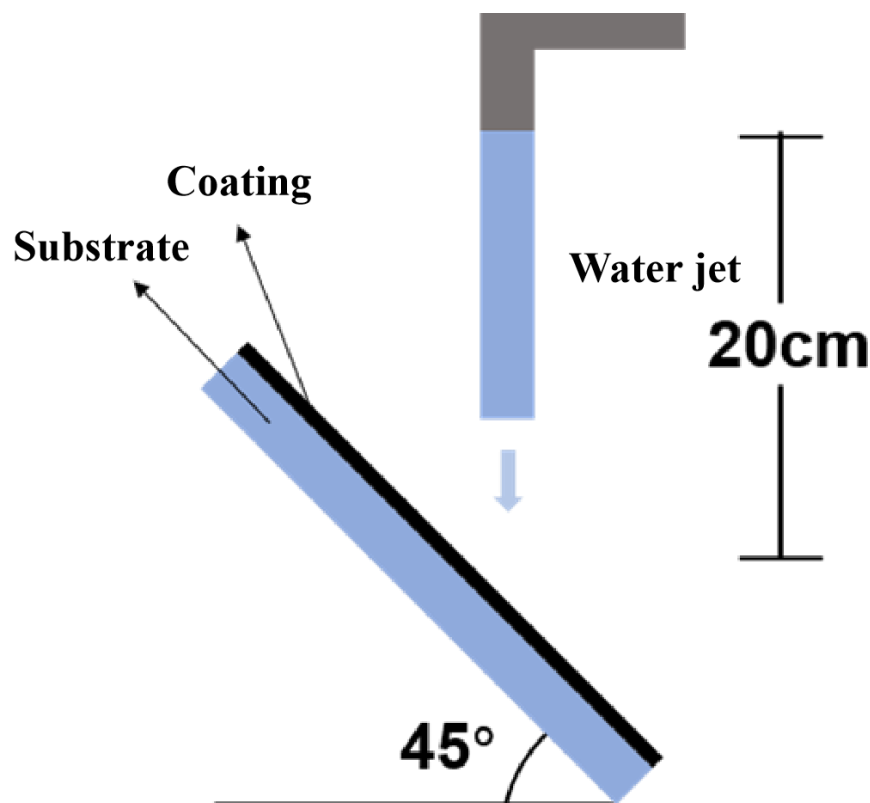


**Figure 3.** Schematic diagram of running water impact test.

To evaluate the chemical durability of the coatings, the samples were immersed in different corrosive solutions with pH values of 0, 1, 13, and 14 at room temperature. The pH was adjusted using sodium hydroxide or sulfuric acid. The change in WCA of the coating surfaces was recorded every 24 h.

### 3. Results and Discussion

#### 3.1. Surface Morphologies and Chemical Compositions

Figure 4a,b show the surface and cross-section morphology of the CS samples. The CS layer presents a uniform porous network, which is a key parameter affecting water wetta-

bility. However, the fragile soot particles are formed by weak van der Waals interactions, and the network can be easily destroyed by the deposition of water droplets. Figure 4c,d show the surface and cross-section morphology of the PDMS-CS sample. The CS network was directly modified by a thin layer of PDMS, improving the adhesive strength of CS networks. Figure 4e,f show the surface and cross-section morphology of the PET-CS samples. When the PET powders were subjected to a candle flame that possessed a temperature higher than the melting point of PET, the applied heat caused the PET powders to melt during the deposition of CS particles. Therefore, CS particles were embedded in the PET matrix, forming a PET-wrapped porous nanostructure. PET powders, acting as binders, built bridges between the CS particles, resulting in the agglomeration of soot particles. After cooling, PET-wrapped CS networks formed agglomerated nanostructures, presenting loofah-like micro-nanostructures [22]. This specific micro-nanostructure was formed under the double actions of the molecular interaction of melted PET and the self-assembly of CS particles.

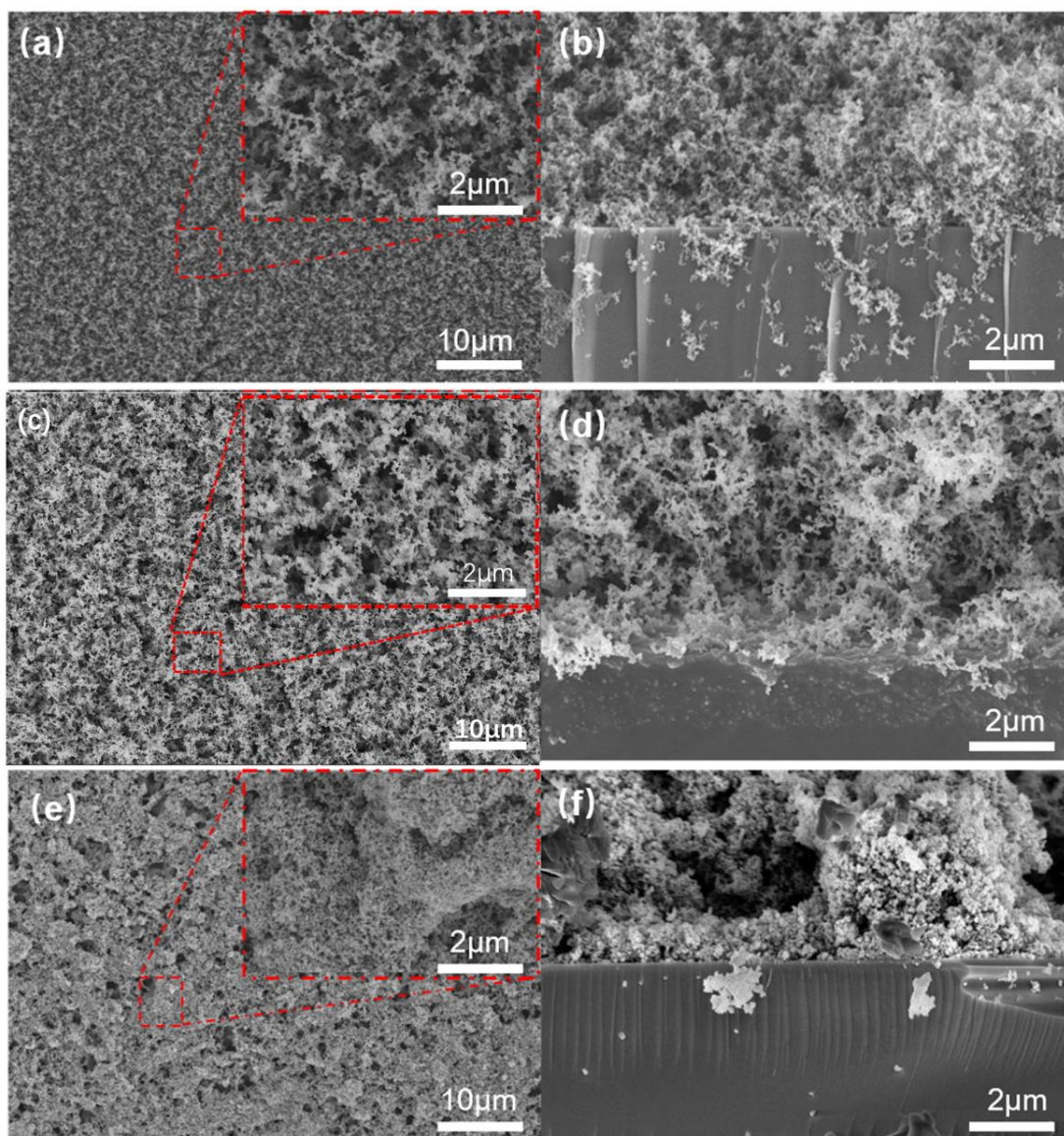


**Figure 4.** Surface morphology and cross-section of (a,b) CS samples, (c,d) PDMS-CS samples, and (e,f) PET-CS samples. The top-right insets show the corresponding high magnification FESEM images.

Figure 5 shows the FTIR spectra of the PDMS-CS and PET-CS surfaces. In Figure 5a, the sharp peaks at  $803\text{ cm}^{-1}$  were assigned to Si-C stretching of Si-CH<sub>3</sub> in PDMS. The band absorption peak at  $1095\text{ cm}^{-1}$  was due to Si-O-Si stretching in the structure of PDMS. The peaks at  $1262\text{ cm}^{-1}$  and  $2965\text{ cm}^{-1}$  are attributed to the vibration of -CH<sub>3</sub> symmetric deformation and asymmetric -CH<sub>3</sub> stretching of Si-CH<sub>3</sub> in PDMS, respectively. The most distinctive feature of PDMS is its characteristic Si-O-Si bond stretching vibration peak at  $1095\text{ cm}^{-1}$  in the infrared spectrum [23]. A number of absorption bands of PET are often evident by IR in the range of  $1800\text{ cm}^{-1}$  to  $700\text{ cm}^{-1}$ , as shown in Figure 5b. This region is known as the fingerprint region [24]. The C-O stretching bond of the ester group was evidenced at  $1110\text{ cm}^{-1}$  and  $1266\text{ cm}^{-1}$  in the fingerprint region. The stretching vibration of the C=O bond of the ester group exhibited a strong band at  $1717\text{ cm}^{-1}$ . The C-C phenyl ring stretching showed a band at  $1406\text{ cm}^{-1}$ . Both the PDMS-CS and PET-CS samples contained CS. The small peak at  $1635\text{ cm}^{-1}$  was due to the C=O stretching mode of aromatic or unsaturated carbon bonds. Other peaks at  $1158\text{ cm}^{-1}$  and  $1110\text{ cm}^{-1}$  were due to -C-O stretching. These peaks indicate the presence of hydrocarbon or functional group with elemental carbon during the atmospheric combustion of the candle [25]. The broad peak at  $3447\text{ cm}^{-1}$  was due to the hydrogen-bonded -OH stretching [21].

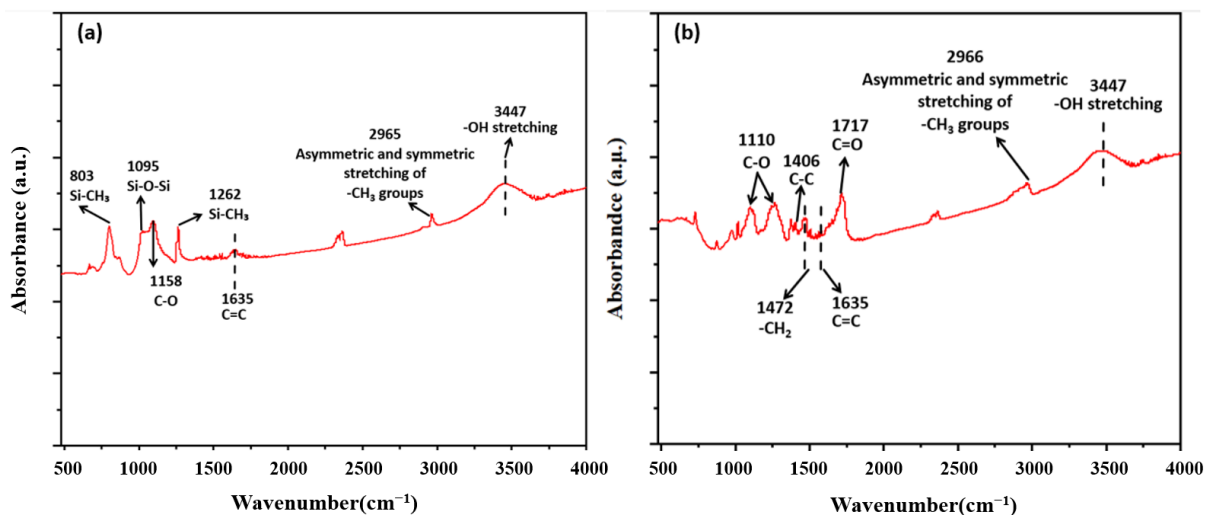


**Figure 5.** FTIR spectra of (a) PDMS-CS samples and (b) PET-CS samples.

### 3.2. Surface Wettability of the Coatings

The measured contact angles of the three superhydrophobic coatings are shown in Figure 6. The CS samples display a WCA of  $161^\circ$ , as shown in Figure 6a. The corresponding RA is  $4^\circ$ , as shown in Figure 6d. The PDMS-CS samples present WCA of  $159^\circ$  and RA of  $4^\circ$ , as shown in Figure 6b,e. Figure 6c,f show the WCA and RA of PET-CS samples, which are  $158^\circ$  and  $5^\circ$ , respectively. All three types of coatings demonstrate superhydrophobicity due to the existence of CS particles [21]. The CS coatings are very fragile, and the superhydrophobic layer can be easily destroyed by water dripping. In comparison, the CS particles in the other two types of coatings were fixed by PDMS and PET. A high-speed flow of running water ( $4\text{ m/s}$ ) can only remove the weak-bonding CS particles during sample preparation, indicating their robust superhydrophobicity.

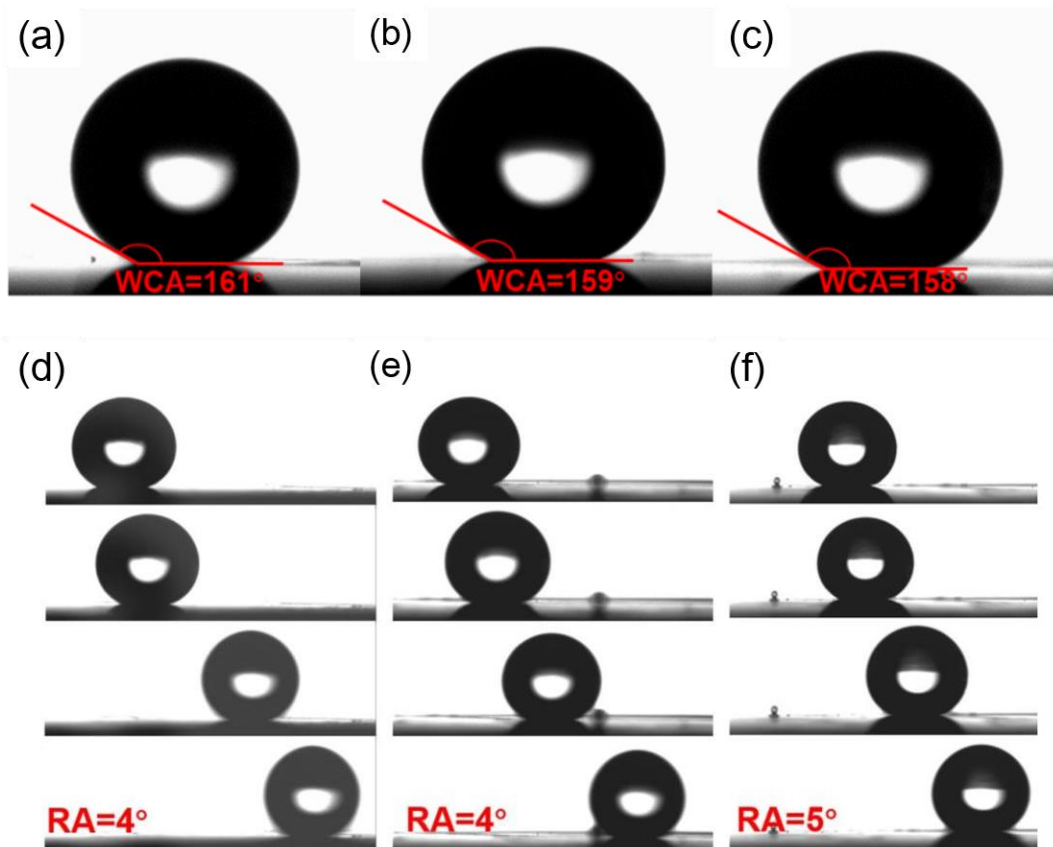


**Figure 6.** The WCA of (a) the CS samples, (b) PDMS-CS samples, and (c) PET-CS samples. The video clips of 10  $\mu$ L droplets rolled off (d) CS, (e) PDMS-CS, and (f) PET-CS coating surfaces.

### 3.3. Underwater Stability

To examine the underwater stability of the three types of superhydrophobic coatings, the prepared samples were placed in a self-designed water-filled glass tube at depths of 80 cm and 140 cm, respectively. The WCA of the samples at different depths was recorded every 24 h. When the CS samples were immersed in water at a depth of 80 cm, the CS network was destroyed immediately, with the CS particles detached gradually from the glass substrate. The results are consistent with our previous report [21]. When the PDMS-CS and PET-CS samples were submerged in an underwater environment, the trapped air would remain in the porous nanostructure and block water from entering the micro-nano structure cavity, forming a stable gas–liquid interface. However, the WCA of the PDMS-CS and PET-CS coatings presented a continuously declining trend as immersion duration increased, as shown in Figure 7. This is due to the action of water pressurization, evaporation, air diffusion, and so on, which leads to the instability of the air-trapping sites and prompts the transition from the Cassie–Baxter state to the Wenzel state. Water gradually destroys the stable gas–liquid interface of the PDMS-CS and PET-CS coatings, resulting in a decrease in WCA. Once the coating surface is wetted, the WCA of the coating surfaces becomes lower than  $150^\circ$  according to our previous study [21].

After 20 days of immersion, the PDMS-CS samples lost superhydrophobicity with WCAs of less than  $150^\circ$  at a depth of 80 cm. The PET-CS sample lost superhydrophobicity after 25 days of immersion which is better than the PDMS-CS sample (Figure 7a). The changes in WCA of the PDMS-CS and PET-CS coatings at a depth of 140 cm are shown in Figure 7b. The same trend was observed as the coatings were continuously immersed in an underwater environment. The WCA of PDMS-CS coatings reduced to about  $148^\circ$  after 16 days of immersion, and parts of the coating surface were wetted. In comparison, the WCA of PET-CS samples was reduced to about  $150^\circ$  after 18 days of immersion. However, the coating surface remained dry, indicating the durability of the PET-CS sam-

ples [21]. With an increase in immersion depth, the underwater stability of the samples decreased gradually.

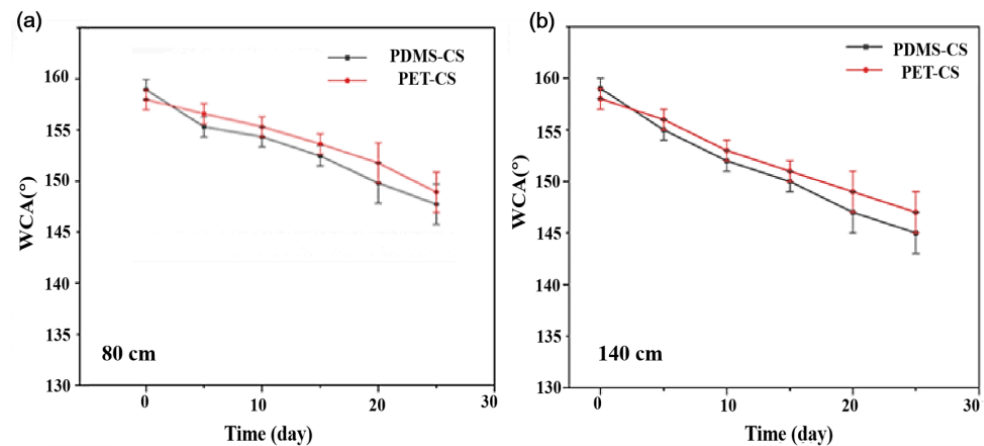


**Figure 7.** The correlation of immersion time and WCAs of PDMS-CS and PET-CS samples in an underwater environment at depths of (a) 80 cm and (b) 140 cm.

The results showed that the superhydrophobicity of PDMS-CS samples and PET-CS samples was maintained for 20 and 25 days at a depth of 80 cm, respectively. At a depth of 140 cm, the superhydrophobicity of PDMS-CS samples and PET-CS samples was maintained for 16 and 18 days, respectively. The PET-CS samples demonstrate superior underwater stability compared to the PDMS-CS samples.

### 3.4. Sandpaper Scratching Test and Analysis

Figure 8 presents the sandpaper abrasion test of the CS, PDMS-CS, and PET-CS coatings. The CS coatings were removed after one abrasion cycle as shown in Figure 8a, resulting in a hydrophilic surface with a WCA of  $\sim 35^\circ$ . The results of the sandpaper abrasion test of the PDMS-CS sample and the PET-CS sample are shown in Figure 8b,c. After three abrasion cycles, a large piece of the coating was scratched off from the surface of the PDMS-CS samples, and the CS network was completely destroyed after five abrasion cycles (about 100 cm), leaving a microstructured PDMS-CS layer and obvious scratches, as shown in Figure 8d. The WCAs of PDMS-CS samples decreased significantly as the abrasion cycles increased, as shown in Figure 8f. The PET-CS coatings show excellent mechanical stability. The PET-CS coating surfaces present superhydrophobicity after about 40 abrasion cycles (8 m), as shown in Figure 8c. Figure 8e displays the SEM images of the PET-CS coating surfaces after 45 abrasion cycles. Although obvious scratches were also observed on the surface, and parts of the loofah-like micro-nanostructures were damaged, the agglomerated nanostructures which were formed by the PET-wrapped CS particles were retained. That is the reason why the PET-CS coating could maintain its superhydrophobicity after about 40 abrasion cycles (8 m). The excellent mechanical stability of the PET-CS coating is due to the stiffness of PET and the highly bonded PET and CS nanoparticles, which are not easy to be damaged under the continuous action of external force.

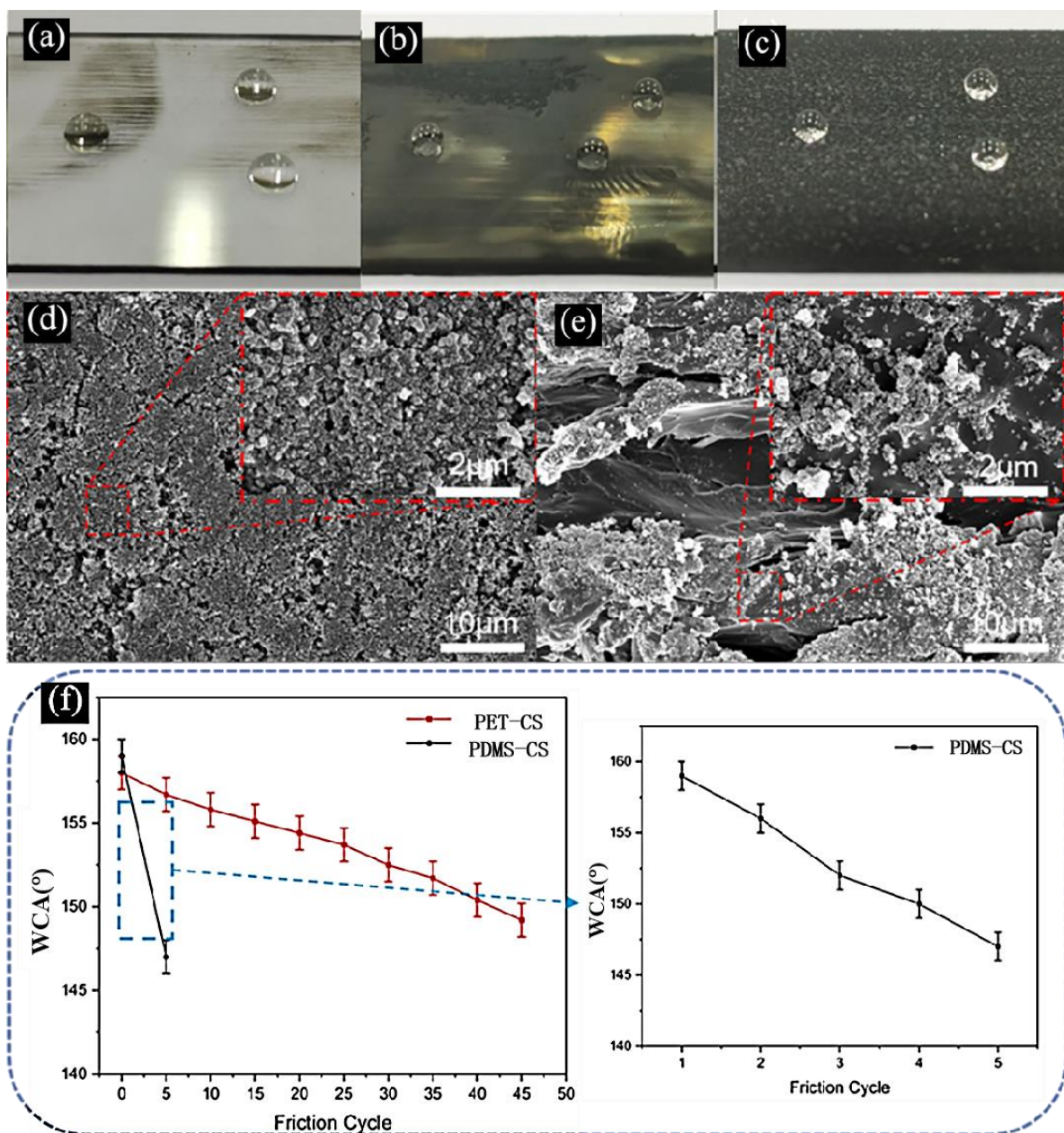


**Figure 8.** The sandpaper abrasion test of the (a) CS samples after 1 abrasion cycle, (b) PDMS-CS samples after 5 abrasion cycles, and (c) PET-CS samples after 40 abrasion cycles. SEM images of the (d) PDMS-CS and (e) PET-CS coating surfaces after 5 and 45 abrasion cycles, respectively. Special emphasis was given to the residue CS networks of each type of samples after the abrasion test. (f) The change in WCA over abrasion cycles of the PET-CS coatings and PDMS-CS coatings. The inset is an enlarged image of the WCA of PDMS-CS coatings in the dotted square.

### 3.5. Water Impact Tests

The water impact resistance of the coatings is one of the most important properties and is usually evaluated by monitoring changes in the WCA of coating surfaces in relation to the operation time. The tap water impact results are shown in Figure 9. The CS coating surface was easily destroyed, revealing a large piece of the substrate surface (Figure 9a). The PDMS-CS and PET-CS coating surfaces could withstand the impact of running tap water at a flow velocity of 2 m/s and performed well initially. After an operation time of 4 min, parts of the PDMS-CS coatings peeled off, as marked in the yellow oval in Figure 9b. The superhydrophobicity of the PDMS-CS coating surfaces disappeared, with a WCA of

less than  $150^\circ$  after an operation time of 8 min, and the corresponding SEM image of the PDMS-CS coating surfaces is shown in Figure 9d. It can be seen that the amount of CS network is significantly reduced, resulting in reduced hydrophobicity. In comparison, the PET-CS coatings retained loofah-like micro-nanostructures within an operation time of 13 min and presented a WCA of higher than  $150^\circ$  and a RA of less than  $10^\circ$  (Figure 9c,e). Although parts of the CS particles on the coating surface were washed away, agglomerated CS particles preserved micro-nanostructures, as highlighted in Figure 9e, indicating their improved durability. This was mainly due to the good mechanical, thermal, and chemical resistance of the semi-crystalline PET. The PET-CS coatings displayed superior sandpaper scratching and water-impacting resistance to the PDMS-CS coatings and other reported coatings [26–30].

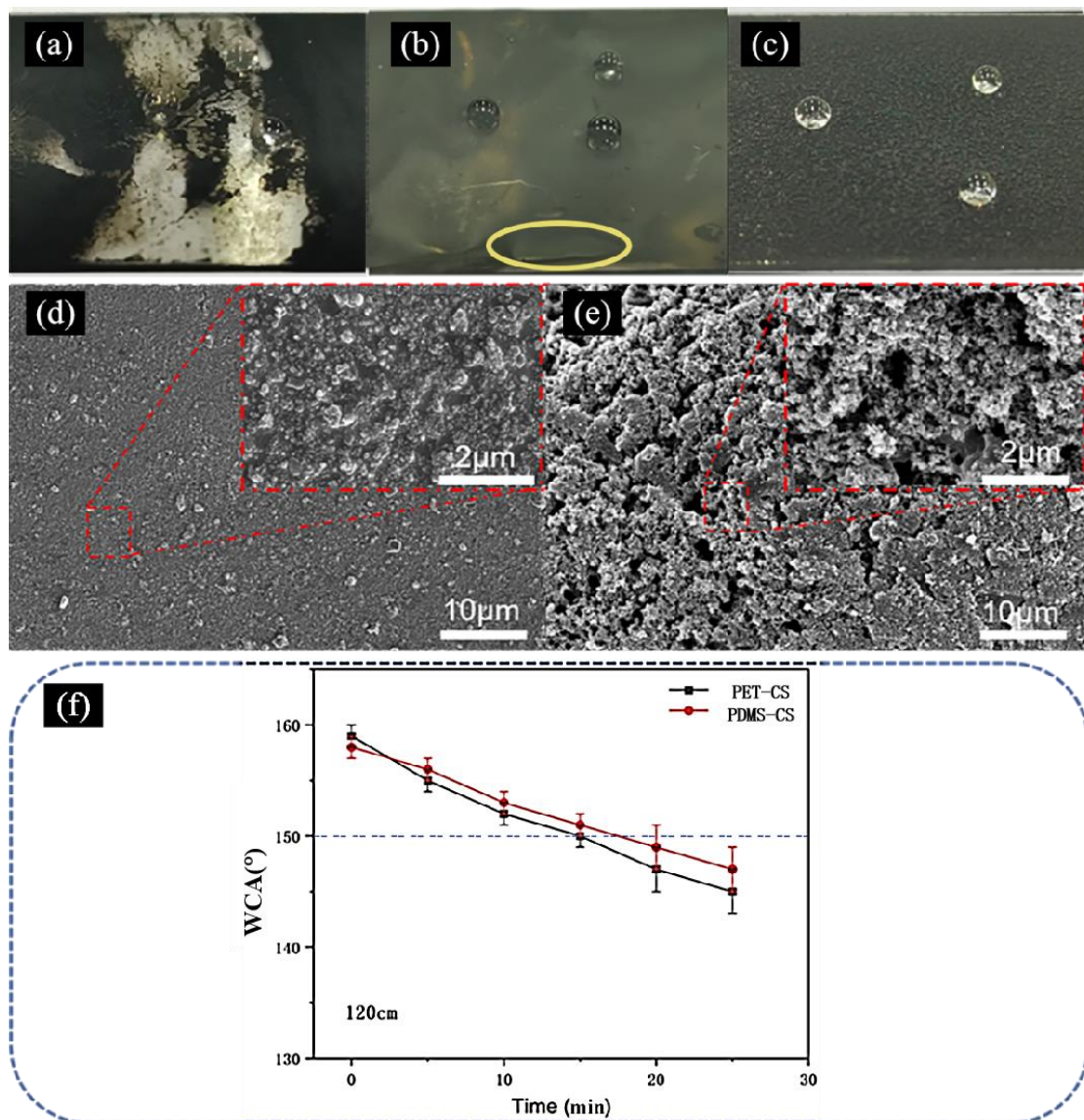


**Figure 9.** The water impact test of the (a) CS, (b) PDMS-CS, and (c) PET-CS samples. The peeled-off parts of the PDMS-CS coatings is marked in the yellow oval. SEM images of the (d) PDMS-CS and (e) PET-CS coating surfaces after operation time of 8 min and 13 min, separately. Special emphasis was given to the residue CS networks after the water impact test. (f) The change in WCA over time of the PDMS-CS and PET-CS coatings.

### 3.6. Chemical Durability

To examine the chemical stability of the PDMS-CS and PET-CS coating surfaces, the samples were immersed in different solutions with pH equal to 1, 2, 13, and 14 at room temperature, respectively. The WCA of the PDMS-CS and PET-CS coating surfaces was recorded every 5 days as shown in Figure 10. The WCA of PDMS-CS coatings decreased continuously over immersion time in different solutions (Figure 10a). The solution with pH = 14 and 13 broke the bonds of the PDMS-CS surfaces during 5 days of immersion. The superhydrophobicity of the PDMS-CS coatings was destroyed with WCA values less than 140°. The PDMS-CS coatings could withstand acid attacks with pH values of 1 and 2 for 5 days and 10 days, respectively. The coatings displayed better resistance towards acid than alkali. The chemical stability of the PET-CS coating surfaces is shown in Figure 10b. Although the solution with a pH value of 14 broke the chemical bonds of the PET-CS surfaces during 5 days of immersion [31], the coating maintained its superhydrophobicity after 20 days of immersion in different solutions with pH values of 1, 2, and 13, demonstrating its good chemical stability.

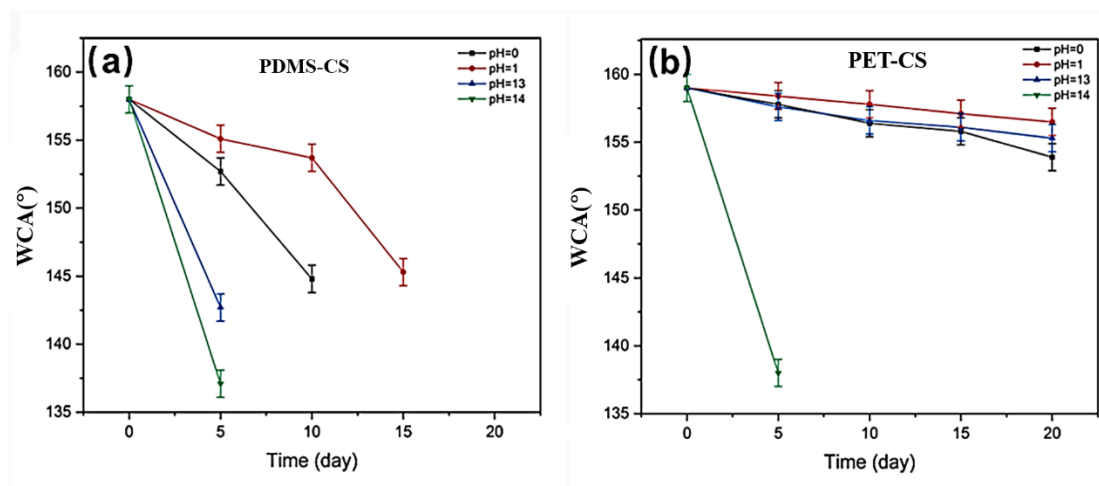


**Figure 10.** (a) The WCA change in (a) PDMS-CS and (b) PET-CS samples over time after being submerged in different pH solutions.

## 4. Conclusions

In this study, a PET-wrapped CS superhydrophobic surface was developed. The obtained surface displays superhydrophobicity, underwater stability, mechanical durability, dynamic impact resistance, and chemical resistance. It has been proven that the PET-wrapped CS loofah-like micro-nanostructures exhibit good water repellence under various pressures. The addition of PET protects the CS networks and successfully improves the mechanical stability, adhesion to substrates, and dynamic impact resistance of the coatings. The excellent water resistance also enables its chemical resistance. The developed coatings hold great promise for applications in marine engineering and offshore constructions.

**Author Contributions:** X.W.; methodology, supervision, writing—original draft preparation, Z.H.; validation, Z.H. and Y.W.; formal analysis and investigation, Y.P.; resources, X.J.; project administration. All authors have read and agreed to the published version of the manuscript.

**Funding:** National Natural Science Foundation of China under Grant (52005109) and the Project of Smart Medical Innovation and Technology Center of Guangdong University of Technology.

**Data Availability Statement:** The data presented in this study are available in this article.

**Conflicts of Interest:** There are no conflicts of interest to declare.

## References

1. Marmur, A. Underwater superhydrophobicity: Theoretical feasibility. *Langmuir* **2006**, *22*, 1400–1402. [[CrossRef](#)]
2. Yu, N.; Li, Z.R.; McClelland, A.; Kim, C.J.C. Combined theory and experimental verification of plastron stability on superhydrophobic surface. In Proceedings of the 2022 IEEE 35th International Conference on Micro Electro Mechanical Systems Conference (MEMS), Tokyo, Japan, 9–13 January 2022; IEEE: Piscataway Township, NJ, USA, 2022; pp. 99–101. [[CrossRef](#)]
3. Smyrnakis, A.; Ioannou, D.; Ellinas, K.; Tserepi, A.; Gogolides, E. Real-Time Monitoring and Quantification of Underwater Superhydrophobicity. *Adv. Mater. Interfaces* **2022**, *9*, 2101393. [[CrossRef](#)]
4. Xiang, Y.; Huang, S.; Lv, P.; Xue, Y.; Su, Q.; Duan, H. Ultimate stable underwater superhydrophobic state. *Phys. Rev. Lett.* **2017**, *119*, 134501. [[CrossRef](#)]
5. Breveleri, J.; Mohammadshahi, S.; Dunigan, T.; Ling, H. Plastron restoration for underwater superhydrophobic surface by porous material and gas injection. *Colloids Surf. A Physicochem. Eng. Asp.* **2023**, *676*, 132319. [[CrossRef](#)]
6. Xiang, Y.; Huang, S.; Huang, T.Y.; Dong, A.; Cao, D.; Li, H.; Duan, H. Superrepellency of underwater hierarchical structures on *Salvinia* leaf. *Proc. Natl. Acad. Sci. USA* **2020**, *117*, 2282–2287. [[CrossRef](#)]
7. Choi, W.; Kang, M.; Park, J.Y.; Jeong, H.E.; Lee, S.J. Enhanced air stability of superhydrophobic surfaces with flexible overhangs of re-entrant structures. *Phys. Fluids* **2021**, *33*, 022001. [[CrossRef](#)]
8. Deepak, J.; Arindam, D. Longevity of plastron layer in underwater vapor stable superhydrophobic surfaces under different atmospheric condition and drag measurements. *Bull. Am. Phys. Soc.* **2022**, *67*, 19.
9. Dai, Z.; Ding, S.; Lei, M.; Li, S.; Xu, Y.; Zhou, Y.; Zhou, B. A superhydrophobic and anti-corrosion strain sensor for robust underwater applications. *J. Mater. Chem. A* **2021**, *9*, 15282–15293. [[CrossRef](#)]
10. Ni, Y.; Huang, J.; Li, S.; Dong, X.; Zhu, T.; Cai, W.; Lai, Y. Robust superhydrophobic rGO/PPy/PDMS coatings on a polyurethane sponge for underwater pressure and temperature sensing. *ACS Appl. Mater. Interfaces* **2021**, *13*, 53271–53281. [[CrossRef](#)]
11. Nazhipkyzy, M.; Nurgain, A.; Florent, M.; Policicchio, A.; Bandosz, T.J. Magnetic soot: Surface properties and application to remove oil contamination from water. *J. Environ. Chem. Eng.* **2019**, *7*, 103074. [[CrossRef](#)]
12. Esmeryan, K.D.; Ganeva, R.R.; Stamenov, G.S.; Chaushev, T.A. Superhydrophobic soot coated quartz crystal microbalances: A novel platform for human spermatozoa quality assessment. *Sensors* **2019**, *19*, 123. [[CrossRef](#)] [[PubMed](#)]
13. Yuan, L.; Tao, Y.; Chen, J.; Dai, J.; Song, T.; Ruan, M.; Wang, Z.L. Carbon nanoparticles on carbon fabric for flexible and high-performance field emitters. *Adv. Funct. Mater.* **2011**, *21*, 2150–2154. [[CrossRef](#)]
14. Yuan, L.; Dai, J.; Fan, X.; Song, T.; Tao, Y.T.; Wang, K.; Wang, Z.L. Self-cleaning flexible infrared nanosensor based on carbon nanoparticles. *ACS Nano* **2011**, *5*, 4007–4013. [[CrossRef](#)] [[PubMed](#)]
15. Iqbal, R.; Majhy, B.; Sen, A.K. Facile fabrication and characterization of a PDMS-derived candle soot coated stable biocompatible superhydrophobic and superhemophobic surface. *ACS Appl. Mater. Interfaces* **2017**, *9*, 31170–31180. [[CrossRef](#)]
16. Zhao, F.; Liu, L.; Ma, F.; Liu, L. Candle soot coated nickel foam for facile water and oil mixture separation. *RSC Adv.* **2014**, *4*, 7132–7135. [[CrossRef](#)]
17. Do, V.T.; Tran, N.G.; Chun, D.M. Fabrication of robust superhydrophobic micro-nano hierarchical surface structure using compression molding with carbon soot nanoparticles and thermoplastic polymer. *Polymer* **2022**, *251*, 124893. [[CrossRef](#)]
18. Esmeryan, K.D.; Castano, C.E.; Bressler, A.H.; Abolghasemibizaki, M.; Mohammadi, R. Rapid synthesis of inherently robust and stable superhydrophobic carbon soot coatings. *Appl. Surf. Sci.* **2016**, *369*, 341–347. [[CrossRef](#)]
19. Liu, X.; Xu, Y.; Ben, K.; Chen, Z.; Wang, Y.; Guan, Z. Transparent, durable and thermally stable PDMS-derived superhydrophobic surfaces. *Appl. Surf. Sci.* **2015**, *339*, 94–101. [[CrossRef](#)]
20. Celik, N.; Kiremitler, N.B.; Ruzi, M.; Onses, M.S. Waxing the soot: Practical fabrication of all-organic superhydrophobic coatings from candle soot and carnauba wax. *Prog. Org. Coat.* **2021**, *153*, 106169. [[CrossRef](#)]
21. Wu, X.; Xiao, M.; Zhang, J.; Tan, G.; Pan, Y.; Lai, Y.; Chen, Z. An underwater stable superhydrophobic surface for robust ultra-long-lasting biofouling resistance. *Chem. Eng. J.* **2023**, *462*, 142091. [[CrossRef](#)]
22. Chen, Y.; Su, N.; Zhang, K.; Zhu, S.; Zhao, L.; Fang, F.; Ren, L.; Guo, Y. In-depth analysis of the structure and properties of two varieties of natural luffa sponge fibers. *Materials* **2017**, *10*, 479. [[CrossRef](#)] [[PubMed](#)]
23. Johnson, L.M.; Gao, L.; Shields, C.W.; Smith, M.; Efimenko, K.; Cushing, K.; Genzer, J.; López, G.P. Elastomeric microparticles for acoustic mediated bioseparations. *J. Nanobiotechnol.* **2013**, *11*, 1–8. [[CrossRef](#)] [[PubMed](#)]
24. El-Saftawy, A.A.; Elfalaky, A.; Ragheb, M.; Zakhary, S. Electron beam induced surface modifications of PET film. *Radiat. Phys. Chem.* **2014**, *102*, 96–102. [[CrossRef](#)]
25. Esmeryan, K.D.; Castano, C.E.; Mohammadi, R. Interactions of superhydrophobic carbon soot coatings with short alkyl chain alcohols and fluorocarbon solutions. *Colloids Surf. A Physicochem. Eng. Asp.* **2017**, *529*, 715–724. [[CrossRef](#)]
26. Yang, L.; Fu, H.; Yang, C.; Tian, W.; Wu, P.; Jiang, W. Carbon soot with arbitrary wettability deposited on solid surface by ethanol flame method. *Colloids Surf. A Physicochem. Eng. Asp.* **2019**, *578*, 123576. [[CrossRef](#)]
27. Sutar, R.S.; Latthe, S.S.; Sargar, A.M.; Patil, C.E.; Jadhav, V.S.; Patil, A.N.; Xing, R. Spray deposition of PDMS/candle soot nps composite for self-cleaning superhydrophobic coating. *Macromol. Symp.* **2020**, *393*, 2000031. [[CrossRef](#)]
28. Lin, X.; Park, S.; Choi, D.; Heo, J.; Hong, J. Mechanically durable superhydrophobic PDMS-candle soot composite coatings with high biocompatibility. *J. Ind. Eng. Chem.* **2019**, *74*, 79–85. [[CrossRef](#)]
29. Chen, B.; Zhang, R.; Fu, H.; Xu, J.; Jing, Y.; Xu, G.; Hou, X. Efficient oil–water separation coating with robust superhydrophobicity and high transparency. *Sci. Rep.* **2022**, *12*, 2187. [[CrossRef](#)] [[PubMed](#)]

30. Li, F.; Liu, Y.; Zhou, H.; Tian, G. Preparation and evaluation of PDMS/carbon soot particles superhydrophobic biomimetic composite coating with self-cleaning and durability. *Biomimetics* **2022**, *7*, 132. [[CrossRef](#)]
31. Xue, C.H.; Zhang, P.; Ma, J.Z.; Ji, P.T.; Li, Y.R.; Jia, S.T. Long-lived superhydrophobic colorful surfaces. *Chem. Commun.* **2013**, *49*, 3588–3590. [[CrossRef](#)]

**Disclaimer/Publisher’s Note:** The statements, opinions and data contained in all publications are solely those of the individual author(s) and contributor(s) and not of MDPI and/or the editor(s). MDPI and/or the editor(s) disclaim responsibility for any injury to people or property resulting from any ideas, methods, instructions or products referred to in the content.